

Prototyping an End-to-End Multi-Modal Tiny-CNN for Cardiovascular Sensor Patches

Mustafa Fuad Rifet Ibrahim, Tunc Alkanat, Maurice Meijer,
Felix Manthey, Alexander Schlaefer, Peer Steldinger

Abstract—The vast majority of cardiovascular diseases may be preventable if early signs and risk factors are detected. Cardiovascular monitoring with body-worn sensor devices like sensor patches allows for the detection of such signs while preserving the freedom and comfort of patients. However, the analysis of the sensor data must be robust, reliable, efficient, and highly accurate. Deep learning methods can automate data interpretation, reducing the workload of clinicians. In this work, we analyze the feasibility of applying deep learning models to the classification of synchronized electrocardiogram (ECG) and phonocardiogram (PCG) recordings on resource-constrained medical edge devices. We propose a convolutional neural network with early fusion of data to solve a binary classification problem. We train and validate our model on the synchronized ECG and PCG recordings from the Physionet Challenge 2016 dataset. Our approach reduces memory footprint and compute cost by three orders of magnitude compared to the state-of-the-art while maintaining competitive accuracy. We demonstrate the applicability of our proposed model on medical edge devices by analyzing energy consumption on a microcontroller and an experimental sensor device setup, confirming that on-device inference can be more energy-efficient than continuous data streaming.

Index Terms—edge computing, patient monitoring, sensor patches, smart sensing, tiny-ml

I. INTRODUCTION

Cardiovascular diseases (CVDs) are the leading cause of death globally [1]. Early detection of CVDs or associated

Date of submission: 21 October 2025. This work was supported by the Bundesministerium für Bildung und Forschung (BMBF) under the project 16KISK221 ("Holistische Entwicklung leistungsfähiger 6G-Vernetzung für verteilte medizintechnische Systeme (6G-Health)").

Mustafa Fuad Rifet Ibrahim is with CTO's System Innovation of NXP Semiconductors Germany GmbH, Hamburg, Germany (e-mail: mustafa.ibrahim@nxp.com) and Institute of Medical Technology and Intelligent Systems, Hamburg University of Technology, Hamburg, Germany and Department of Informatics, Hamburg University of Applied Sciences, Hamburg, Germany.

Tunc Alkanat is with Advanced Chip Engineering division of NXP Semiconductors, Eindhoven, The Netherlands (e-mail: tunc.alkanat@nxp.com).

Maurice Meijer is with Business Line Secure Connected Edge of NXP Semiconductors, Eindhoven, The Netherlands (e-mail: maurice.meijer@nxp.com).

Felix Manthey is with CTO's System Innovation of NXP Semiconductors Germany GmbH, Hamburg, Germany (e-mail: felix.manthey@nxp.com).

Alexander Schlaefer is with Institute of Medical Technology and Intelligent Systems, Hamburg University of Technology, Hamburg, Germany (e-mail: schlaefer@tuhh.de).

Peer Steldinger is with Department of Informatics, Hamburg University of Applied Sciences, Hamburg, Germany (e-mail: Peer.Steldinger@haw-hamburg.de).

risk factors significantly improves the efficacy of preventive measures [2], [3]. Continuous monitoring is essential for early detection, and combining modalities, such as electrocardiograms (ECGs) and phonocardiograms (PCGs), can enhance diagnostic performance. To minimize the impact on daily activities, monitoring devices must be lightweight. However, deploying such devices generates vast amounts of data, necessitating automated processing. Deep learning (DL) provides models that can analyze this data and has been shown to yield improved performance in the analysis of ECG and PCG data [4], [5]. However, this performance increase comes at the expense of computational and energy costs, hindering adoption in portable medical applications. While cloud or hub devices (e.g., smartphones) can provide the computational power for DL, remote processing introduces privacy concerns, transmission energy costs, and potential service disruptions. We focus on executing the DL model directly on the monitoring device. Transmission is only required upon detecting an anomaly which reduces energy consumption, enhances privacy and allows for continuous and independent monitoring. However, computing on the sensor also comes with very tight constraints on memory footprint, computational cost and energy consumption. Low energy consumption enables longer battery life or smaller batteries, improving patient comfort. In this work, we propose an efficient end-to-end convolutional neural network (CNN) [6] using an efficient CNN building block. We analyze its classification performance by applying it to a public dataset containing synchronized ECG and PCG recordings. We achieve competitive accuracy compared to the state-of-the-art and a reduction in parameter count and Floating Point Operations (FLOPs) of three orders of magnitude. This work is an extension to our previous work [7] in which we approximated the hardware requirements of our proposed CNN model by simulation. In the present work, we compare classification performance of our model with other popular DL architectures and analyze it with respect to energy consumption while running on a microcontroller and an experimental sensor device setup to get a more accurate assessment of the efficiency of deep learning models on sensor patch hardware. The remainder of this paper is organized as follows. In Section II, we briefly review the related work. In Section III, we describe our method in detail. In Sections IV and V, we describe the experimental setup and present results on the classification performance of our method and the efficiency, respectively. In Section VI, we discuss the performance and efficiency results. Finally, in Section VII, we

give concluding remarks.

II. RELATED WORK

A. ECG-/PCG-Based Anomaly Detection

Various ML-based solutions for the classification of ECG and PCG signals have been proposed. Approaches, such as [8], focused on traditional ML methods involving explicit segmentation of cardiac cycles and extensive feature engineering (e.g., time, frequency, statistical features), followed by classifiers such as logistic regression and support vector machines (SVM) [9]. Recent works have increasingly utilized DL. A common strategy involves transforming 1D signals into 2D representations to leverage architectures designed for image data. This includes converting PCG segments into intensity maps [10], using continuous wavelet transforms (CWT) to generate scalograms [11], or applying techniques like the Gramian Angular Difference Field (GADF) [12]. Notably, transfer learning has been employed to mitigate the scarcity of synchronized multi-modal data [11]. In contrast, other DL approaches process signals directly in the time domain, often using dual-branch 1-D CNNs with feature fusion before the fully connected layers [13]. Hybrid approaches and ensembles have also been explored. These methods combine classic ML pipelines (expert-designed features) with end-to-end DL pipelines (processing raw signals or spectrograms) using a meta-learner [14]. Alternatively, DL models (CNNs and long short-term memory (LSTM) [15]) can serve purely as feature extractors, with subsequent classification performed by SVMs [16]. More complex ensembles combine different architectures (e.g., BiLSTM on 1D data and GoogLeNet on 2D scalograms) using evidence theory for decision fusion [17]. To better capture the interplay between the heart's electrical (ECG) and mechanical (PCG) activities, advanced feature fusion strategies have recently emerged. Architectures like CPDNet [18] and PACFNet [19] utilize three-branch designs (ECG-specific, PCG-specific, and fusion encoders). They employ sophisticated mechanisms such as progressive dense fusion [18] or progressive attention-based cross-modal fusion [19] to integrate features dynamically across multiple hierarchical levels. Efforts toward end-to-end processing, which minimizes pre-processing overhead, have also been made. Thomae et al. [20] developed a small end-to-end model (CNN-GRU with attention) using only the raw PCG signal as input, achieving an average of specificity and sensitivity of 0.55. Our work differs from the aforementioned related works by focusing explicitly on the constraints of wearable edge devices: (1) we propose an efficient end-to-end approach utilizing raw, downsampled signals without costly feature extraction or signal transformation, (2) the proposed model provides state-of-the-art classification performance, and (3) the proposed model is three orders of magnitude less demanding in terms of memory footprint and computational cost compared to the current state-of-the-art model.

B. Remote Cardiovascular Monitoring With Wearables

Recent literature has summarized developments in biosignal acquisition, telemonitoring, and the application of ML in

wearable cardiovascular monitoring. Reviews have covered the use of wearables in heart failure management [21], the integration of novel sensors and algorithms [22], and the accuracy of heart rate monitoring [23]. Several studies specifically analyzed the use of AI and wearables for detecting CVDs and other conditions [24]–[26], highlighting the potential for early diagnosis while discussing associated software and hardware challenges. Other works have implemented and optimized ML solutions for specific cardiovascular use-cases, focusing on performance and efficiency. Several studies explored optimization for general-purpose hardware. Ribeiro et al. [27] analyzed the latency and energy efficiency of a quantized CNN for continuous ECG monitoring on mobile and low-power CPUs (ARM Cortex-A55 and A53). Beyond software optimization, researchers have investigated specialized hardware acceleration and custom designs. Ran et al. [28] employed pruning and quantization to accelerate CNN inference on an FPGA platform, validating their approach with real-time analysis. Lu et al. [29] designed a custom hardware architecture featuring a fully pipelined processing unit array for high efficiency. They evaluated both performance and hardware resource efficiency. Furthermore, Hsieh et al. [30] explored ultra-low power solutions, proposing an analog implementation suitable for battery-less sensor nodes and analyzing aspects such as power consumption. In contrast, systems like that proposed by Jin et al. [31], [32] rely on transmitting wearable data to a smartphone for classification, incorporating clinical data for better adaptivity. Our work differs from the aforementioned related works by one or both of the following aspects: (1) we utilize two sensor modalities, namely ECG and PCG, for improving classification accuracy, (2) we achieve very low energy consumption on a microcontroller and prove this by measurement.

III. METHODOLOGY

Our system (Fig. 1) includes three components: sensing (ECG and PCG), processing (classification) and communication upon anomaly detection. We assume the use of a resource-constrained healthcare sensor patch to run these operations on. All of these operations incur computational cost, memory requirements (silicon area) and energy cost. However, we limit the scope of this section to the analysis of the processing portion of the pipeline, since this is the portion in which our model is applied.

A. Dataset

We utilize the Physionet/Computing in Cardiology Challenge 2016 dataset [33], [34] for this study. As our focus is on analyzing multi-modal cardiovascular data, we specifically use the Massachusetts Institute of Technology heart sounds sub-dataset (designated as "training-a"). This is the only subset within the 2016 challenge that provides synchronized ECG and PCG data. The "training-a" subset contains 409 recordings (405 with synchronized ECG and PCG) from 121 subjects. It is imbalanced, comprising 117 healthy recordings and 288 pathological recordings (mitral valve prolapse, aortic disease and benign murmurs). The recordings, ranging from 9s to 37s

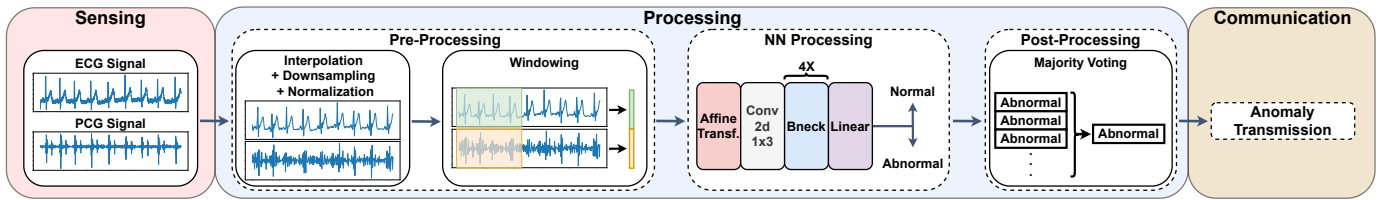


Fig. 1. An overview of the system pipeline [7]. After the ECG and PCG signals are measured the data is interpolated, downsampled and normalized. After that windows are extracted. The windows of ECG and PCG signals are concatenated and fed into our model which classifies them into normal or abnormal. A majority voting over multiple windows gives the final classification. In case of a cardiovascular anomaly the data is transmitted to a doctor.

in length, were captured using a Welch Allyn Meditron electronic stethoscope during in-home visits or in the hospital in an uncontrolled environment. While the dataset documentation specifies the recording device, detailed information regarding the specific ECG leads used or the exact placement is not available. The data was downsampled from 44,100 Hz to 2000 Hz when the challenge dataset was assembled by Liu *et al.* [33]. Crucially, the dataset lacks patient identifiers linking recordings to specific subjects, which imposes limitations on the evaluation strategy, as discussed in Section IV-B.

B. Pre-Processing

First, we use interpolation to fill any missing values in the ECG and PCG signals present in the dataset. Subsequently, to reduce computational costs and energy consumption on the target edge device, we significantly downsample the signals from 2000 Hz. We normalize the signals separately to a mean of 0 and a standard deviation of 1 and extract 3 s windows with an overlap duration of 2 s. We aim for a tensor length suitable for efficient processing, selecting a target length of 128 samples per modality based on a trade-off analysis detailed in Sections IV-C and V-B. Consequently, the required sampling frequency is approximately 42.67 Hz. Finally, we concatenate the two tensors corresponding to the ECG and PCG signals for the same time interval in the width dimension, which yields an input of shape $1 \times 1 \times 256$ (Channels \times Height \times Width). Our network operates end-to-end, requiring no heart beat segmentation or feature extraction, further saving computational resources. In a practical, real-time implementation, the interpolation step used for the offline dataset is unnecessary. Instead, data is continuously gathered from the sensors until the required 256 samples are available for the neural network input window. We use these pre-processing steps for both our proposed CNN and the other DL architectures implemented for comparison.

C. Network Design

Our proposed neural network architecture consists of four parts. The operations and parameters used for our primary configuration (CNN 128) are listed in Table I. In the first part, we use an affine transform layer that allows the network to weight the ECG and PCG portions of the input differently. This is advantageous as the modalities may have differing relevance for classification. To this end, we use separate, trainable shift and scale parameters for the two signal types. We determine

the initial values for these parameters with a simple grid search. In the second part of our network, we use a convolutional layer. For our primary configuration (CNN 128), this layer has a stride of 2, reducing the signal length and thus the computational cost in the subsequent layers. When analyzing the impact of different input signal lengths (see Sections IV-C and V-B), we adapt this first convolutional layer. To ensure fair comparison and manage the receptive field, the kernel size and stride are adjusted so the output length remains constant (128 width) across experiments. This facilitates the capture of relevant temporal patterns while controlling computation regardless of the initial input length. For the third part, we make use of four bottleneck blocks introduced in the MobileNetV2 paper [35]. Bottleneck blocks maintain low dimensionality at the input/output while expanding dimensions during depthwise convolution for higher expressiveness. We utilize this block due to its demonstrated computational efficiency [35], which is crucial for reducing energy consumption on the sensor device. We use the channel numbers and non-linearities of the MobileNetV3-Small architecture [36]. However, instead of 2D convolutions we use 1D convolutions. In order to avoid losing relevant information through excessive downsampling we also change the stride length in the bottleneck blocks to 1. Finally, we use a fully-connected layer with the softmax activation to compute the class scores for the normal and abnormal class. For comparison we also implement a multilayer perceptron (MLP) [37], an LSTM and a transformer model [38] optimized for the same parameter count (for the detailed architecture parameters see Appendix A). For these architectures we also use the affine transform layer initialized in the same way.

D. Post-Processing

To determine the classification result for a recording we use a majority voting scheme over all windows of the same recording. For a practical implementation of our system we propose to redo the majority voting based on the current window and the last $N - 1$ windows. The parameter N affects the sensitivity of the system to short-term fluctuations and so has to be chosen carefully. When a cardiovascular anomaly is detected the data containing the anomaly is transmitted to a doctor for an assessment of the classification result.

IV. MODEL PERFORMANCE

A. Training

We implemented and trained our CNN model using the PyTorch framework [39] on an NVIDIA RTX A6000. Training

TABLE I
NETWORK OPERATIONS AND PARAMETERS

Input	Operator	Exp. size	Non-Linear	Stride
1x1x256	Affine Transform	-	-	-
1x1x256	Conv2d, 1x3	-	HardSwish	2
16x1x128	Bottleneck, 1x3	16	ReLU	1
16x1x128	Bottleneck, 1x3	72	ReLU	1
24x1x128	Bottleneck, 1x3	88	ReLU	1
24x1x128	Bottleneck, 1x5	96	HardSwish	1
40x1x128	Avg. Pool	-	-	-
40x1x1	Linear	-	-	-

was conducted for 300 epochs using the AdamW optimizer [40] and cross-entropy loss. We initialized the learning rate to 10^{-3} and used a batch size of 32. To address the class imbalance inherent in the dataset, we employed weighted random sampling during training. For the comparative DL architectures (MLP, LSTM, transformer), we utilized Optuna [41] to optimize their hyperparameters, maximizing accuracy while maintaining a parameter count similar to our CNN model. The best-performing configuration for each architecture was then trained using the identical protocol as our CNN model.

B. Evaluation

To robustly evaluate the performance and generalization capability of our model, particularly given the relatively small dataset size, we employ 10 times repeated 5-fold cross-validation (CV). A significant challenge with the Physionet 2016 "training-a" dataset is the lack of patient-level identification for each recording. Ideally, data splitting should occur at the patient level. Recordings from the same patient are highly correlated due to unique physiological traits. If learned, these correlations can inflate test scores when the same patient appears in both training and testing sets. Since patient-level splitting is not possible, we cannot guarantee complete patient separation across folds. To mitigate this limitation as effectively as possible, we perform the CV splits at the recording level. This ensures that all windows extracted from a single recording are exclusively assigned to either the training or the testing fold within a given CV iteration. This prevents immediate temporal correlations, arising from factors such as consistent sensor placement, the ambient noise profile, and the short-term physiological state of the patient, from inflating the test scores. While this does not resolve the potential issue of inter-recording correlation from the same patient, it represents the most rigorous evaluation strategy feasible with this dataset. We report the average performance and standard deviations across all 50 runs (10 repetitions x 5 folds). The standard deviation allows us to assess the stability of the model's performance and its sensitivity to specific data partitions. We measure model performance with the following metrics: accuracy, sensitivity, specificity, precision, and F1 score [42]. Additionally, we calculate the area under the receiver operating characteristic curve (AUC) to provide a threshold-independent assessment. We estimate memory cost via parameter count and computational cost via Floating Point Operations (FLOPs). For comparisons with previous works

(Table III), we estimated unreported efficiency metrics by reimplementing the architectures based on their descriptions and analyzing them using the ptflops package [43]. When exact replication was infeasible, we estimated a lower bound by focusing on the computationally dominant portions (e.g., the CNN backbone). These estimations highlight the orders-of-magnitude differences in efficiency rather than providing exact figures.

C. Results

We evaluate the performance of our proposed CNN model by analyzing the impact of input signal length, comparing it with state-of-the-art literature and other lightweight architectures, and performing ablation studies on the input modalities. To determine the optimal balance between performance and computational efficiency, we analyzed the impact of varying the input signal length (Table II). We tested lengths ranging from the original 2000 Hz (6000 samples over 3s) down to 21.33 Hz (64 samples over 3s). As described in Section III-C, the first convolutional layer was adapted in each configuration to maintain a consistent input size for the subsequent bottleneck blocks. The classification performance remains high even with significant downsampling. The model using the full 6000 samples (CNN 6000) achieves the highest accuracy (0.9760), but the models with 1024 samples (CNN 1024) and 128 samples (CNN 128) show only marginal decreases in performance (0.9700 and 0.9705, respectively). Given the substantial reduction in energy consumption achieved by shorter input lengths (discussed in Section V-B), we selected the 128-sample length as the optimal trade-off, providing high accuracy with significantly improved efficiency. All subsequent results are reported using this configuration (CNN 128). We also compare our CNN model against previous works that utilized DL models trained on the same dataset (Table III) and against other common DL architectures optimized for a similar parameter budget (Table IV). It is important to emphasize that the performance metrics reported in the literature (Table III) are derived using heterogeneous evaluation strategies. For instance, some works report accuracy at the segment level [19], while others use a single extracted segment per recording [17] or evaluate at the recording level [11], [18]. Due to these inconsistencies, Table III should not be interpreted as a direct comparison of model efficacy but rather as a contextualization of the performance achieved relative to the computational resources required. As shown in Table III, our CNN model achieves a recording-level accuracy of 0.9705, which is competitive with the results reported by Li Wei Peng et al. [19] (0.9777). Crucially, our model is significantly more efficient. With only 15.9K parameters and 3.72M FLOPs, it achieves a reduction of three orders of magnitude in parameter count and FLOPs compared to the leading model (11.7M parameters, 3.14G FLOPs) and other recent works [12], [13], [17], [18]. Furthermore, Table IV highlights the effectiveness of the CNN architecture which clearly outperforms the MLP, LSTM and transformer models across all metrics. We analyzed the contribution of the two sensor modalities (Table V). The multi-modal approach (ECG + PCG) significantly

TABLE II
CLASSIFICATION RESULTS OF OUR CNN MODEL WITH DIFFERENT INPUT SIGNAL LENGTHS

Model	Accuracy	Sensitivity	Specificity	Precision	F1 Score	AUC
CNN 6000	0.9760 ± 0.0227	0.9854 ± 0.0256	0.9667 ± 0.0377	0.9685 ± 0.0344	0.9764 ± 0.0222	0.9770 ± 0.0260
CNN 1024	0.9700 ± 0.0252	0.9829 +/. 0.0246	0.9572 ± 0.0466	0.9602 ± 0.0412	0.9708 ± 0.0242	0.9725 ± 0.0302
CNN 128	0.9705 ± 0.0246	0.9761 ± 0.0376	0.9650 ± 0.0402	0.9670 ± 0.0363	0.9707 ± 0.0248	0.9695 ± 0.0349
CNN 64	0.9624 ± 0.0257	0.9699 ± 0.0305	0.9549 ± 0.0457	0.9575 ± 0.0416	0.9629 ± 0.0250	0.9644 ± 0.0330

TABLE III
CLASSIFICATION RESULTS COMPARISON WITH PREVIOUS WORKS

Model	Accuracy	Sensitivity	Specificity	Precision	F1 Score	AUC	Params	FLOPs
Li, Wei Peng, et al. (2025)	0.9777	0.9799	0.9728	0.9879	0.9839	0.9967	11.7M	3.14G
Li, Jinghui, et al. (2022)	0.9613	0.9848	0.908	0.9604	0.9724	-	5.8M	3.0G
Morshed, Monjur, and Shaikh Anowarul Fattah. (2023)	0.9506	0.9506	0.9092	0.9508	0.9500	0.99	19.16M	1.69G
Zhang, Haobo, et al. (2024)	0.9441 ± 0.0304	0.9485 ± 0.0514	0.9397 ± 0.0497	-	-	0.973 ± 0.026	25.3M	3.84G
Qi, Pengjia, et al. (2023)	0.9434	0.9769	0.9092	-	-	-	11.25M	2.92G
Li, Pengpai, Yongmei Hu, and Zhi-Ping Liu. (2021)	0.873 ± 0.010	0.903 ± 0.006	0.845 ± 0.018	-	0.874 ± 0.010	0.936 ± 0.011	446K	59.1M
Hettiarachchi, Ramith, et al. (2021)	0.9041	0.9474	0.75	-	-	0.9106	711K	532M
Our CNN	0.9705 ± 0.0246	0.9761 ± 0.0376	0.9650 ± 0.0402	0.9670 ± 0.0363	0.9707 ± 0.0248	0.9695 ± 0.0349	15.9K	3.72M

TABLE IV
CLASSIFICATION RESULTS COMPARISON WITH OTHER NETWORK ARCHITECTURES

Model	Accuracy	Sensitivity	Specificity	Precision	F1 Score	AUC	Params	FLOPs
MLP	0.8290 ± 0.0405	0.8632 ± 0.0842	0.7948 ± 0.0869	0.8144 ± 0.0620	0.8338 ± 0.0414	0.8331 ± 0.0555	16.32K	31.9K
LSTM	0.8333 ± 0.0485	0.8683 ± 0.0992	0.7982 ± 0.0997	0.8206 ± 0.0742	0.8376 ± 0.0517	0.8410 ± 0.0621	15.99K	4.22M
Transformer	0.9282 ± 0.0373	0.9299 ± 0.0666	0.9265 ± 0.0589	0.9306 ± 0.0520	0.9278 ± 0.0383	0.9376 ± 0.0361	16.04K	2.46M
Our CNN	0.9705 ± 0.0246	0.9761 ± 0.0376	0.9650 ± 0.0402	0.9670 ± 0.0363	0.9707 ± 0.0248	0.9695 ± 0.0349	15.9K	3.72M

TABLE V
CLASSIFICATION RESULTS OF OUR CNN MODEL WITH DIFFERENT SENSOR MODALITIES

Model	Accuracy	Sensitivity	Specificity	Precision	F1 Score	AUC
ECG Only	0.9462 ± 0.0293	0.9470 ± 0.0515	0.9454 ± 0.0412	0.9473 ± 0.0380	0.9459 ± 0.0301	0.9516 ± 0.0303
PCG Only	0.7483 ± 0.0429	0.7187 ± 0.1466	0.7780 ± 0.1323	0.7824 ± 0.0815	0.7345 ± 0.0668	0.7047 ± 0.0628
ECG + PCG (no affine)	0.9552 ± 0.0260	0.9745 ± 0.0321	0.9359 ± 0.0545	0.9413 ± 0.0475	0.9565 ± 0.0245	0.9631 ± 0.0297
ECG + PCG (affine)	0.9705 ± 0.0246	0.9761 ± 0.0376	0.9650 ± 0.0402	0.9670 ± 0.0363	0.9707 ± 0.0248	0.9695 ± 0.0349

TABLE VI
CLASSIFICATION RESULTS COMPARISON BETWEEN OUR 8-BIT QUANTIZED AND NON-QUANTIZED CNN MODEL

Model	Accuracy	Sensitivity	Specificity	Precision	F1 Score	AUC
Not Quantized	0.9705 ± 0.0246	0.9761 ± 0.0376	0.9650 ± 0.0402	0.9670 ± 0.0363	0.9707 ± 0.0248	0.9695 ± 0.0349
Quantized	0.9124 ± 0.0378	0.9197 ± 0.0596	0.9051 ± 0.0568	0.9094 ± 0.0503	0.9127 ± 0.0387	0.9204 ± 0.0447

TABLE VII
DETAILS OF THE SENSING AND COMMUNICATION PROCESS OF OUR SENSOR DEVICE SETUP

Parameter	Value
ECG channel bandwidth	500 Hz
Number of ECG channels	1
ECG channel bitwidth	24 bit
BLE package size	213 byte
BLE communication rate	5 packages/second
BLE PHY mode	1 Mbps
BLE Tx power	0 dBm

outperforms single-modality inputs, achieving 0.9705 accuracy compared to 0.9462 for ECG only and 0.7483 for PCG only. The inclusion of the affine transform layer further enhances performance, improving accuracy from 0.9552 to 0.9705, demonstrating the network’s ability to effectively weight the relevance of the two modalities. For the model efficiency analysis in Section V, we quantize our CNN model to 8-Bit using quantization-aware training [44]. As shown in Table VI, the quantized version exhibits a lower accuracy (0.9124) compared to the unquantized version (0.9705). This shows an important trade-off which is further discussed in Section VI.

V. MODEL EFFICIENCY

A. Setup

In our first experiment, we measure the energy consumption per inference and the inference time of our model variants (corresponding to different input signal lengths) on the MCTXN947 evaluation kit (EVK) [45]. The EVK contains both a Cortex-M33 CPU [46] and the eIQ Neutron Neural Processing Unit (NPU) [47], allowing for a comparative analysis. We operate our EVK at 3.3 V. We use the MCU-Link Pro Debug Probe [48] to measure the mean power consumption of the CORE domain [49] which is a collection of circuits that includes the CPU and NPU of the EVK. We measure the mean power consumption during and outside of inference to isolate the power consumption of the model. We calculate the energy consumption per inference from the mean power consumption and the inference time. The model processes 3s windows with 2s overlap, resulting in one inference per second in a live scenario. Thus, the calculated energy per inference equals the mean power consumption over one second. In our second experiment, we use an experimental sensor device setup that is capable of sensing and transmitting ECG data. This setup consists of a custom board with an NHS52S04 chip [50] for wireless data transmission and an SNCE800 chip [51] for ECG sensing (see Fig. 2 for an overview).

Table VII gives more detailed information for the sensing and communication process. We operate our sensor device setup at 3.3 V. We use the MCU-Link Pro Debug Probe to measure the mean power consumption of only the NHS52S04 chip, since it contains the BLE transceiver, both while only sensing and while sensing and transmitting data to measure the additional power consumption of the communication process. We compare the mean power consumption of communication with that of the ML process to evaluate the impact of using on-device ML.

B. Results

We summarize the results of our first experiment, evaluating the impact of input signal length and processor choice, in Table VIII. Across all signal lengths, inference on the NPU is significantly more efficient than on the ARM Cortex-M33. For our chosen model (CNN 128), the inference time on the NPU is 20.36ms compared to 79.76ms on the Cortex-M33 (approximately 3.9 times faster). This leads to an energy per inference of 0.092mJ (NPU) versus 0.639mJ (Cortex-M33), demonstrating the NPU is approximately 6.9 times more energy-efficient. Table VIII also demonstrates the significant impact of input signal length on efficiency. Reducing the input length from 6000 samples to 128 samples drastically reduces the energy per inference on the NPU from 0.216mJ to 0.092mJ, and the inference time from 37.82ms to 20.36ms. This substantial energy saving, combined with the high accuracy maintained by the CNN 128 configuration (Table II), validates our approach of utilizing aggressive downsampling for edge deployment. The results comparing the mean power consumption of the ML inference (using the CNN 128 model) with BLE communication are summarized in Fig. 3. Model inference on the Cortex-M33 (0.629 mW) is significantly more expensive than constant BLE communication (0.198 mW). However, model inference on the NPU (0.09 mW) is more than 53% cheaper than BLE communication.

VI. DISCUSSION

This work provides a proof-of-concept demonstrating the feasibility of applying end-to-end, multi-modal DL models on resource-constrained medical edge devices for cardiovascular monitoring. We present quantitative evidence showing that local processing using an NPU coupled with a lightweight CNN model can be more energy-efficient than constant data transmission. Furthermore, we demonstrate that competitive classification accuracy can be maintained despite significant reductions in model size and input signal resolution.

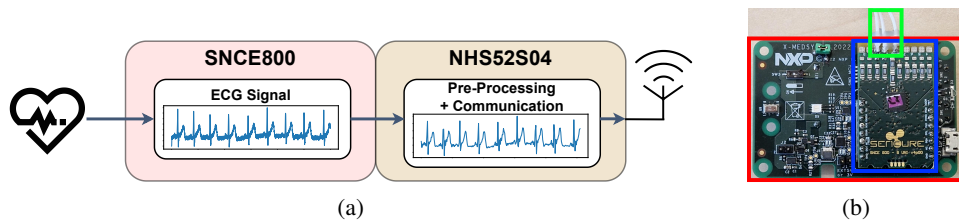


Fig. 2. A schematic and a picture of the hardware components in the setup used for our second experiment described in Section V-A. (a) The measured ECG signal is transmitted from the SNCE800 to the NHS52S04. From there, it is pre-processed with a high-pass, low-pass and notch filter to remove noise before it gets transmitted via BLE to a hypothetical doctor's device which can for example display the ECG data. For simplicity's sake, we skip any intermediary devices or connections between the NHS52S04 and the doctor's device that would be necessary in real life. (b) Red: Custom board with the NHS52S04 chip. Blue: SNCE800 chip. Green: Three ECG electrode cables.

TABLE VIII
EFFICIENCY RESULTS OF OUR CNN MODEL ON THE MCXN-947

Model	CPU: Arm Cortex-M33			NPU: eIQ Neutron		
	Memory Usage [Bytes]	Inference Time [ms]	Energy per Inference [mJ]	Memory Usage [Bytes]	Inference Time [ms]	Energy per Inference [mJ]
CNN 6000	45152	103.06 ± 0.608	0.788 ± 0.010	27968	37.82 ± 0.603	0.216 ± 0.010
CNN 1024	43904	83.13 ± 0.138	0.654 ± 0.008	26752	22.87 ± 0.134	0.115 ± 0.004
CNN 128	43680	79.76 ± 0.088	0.639 ± 0.009	26496	20.36 ± 0.089	0.092 ± 0.003
CNN 64	43680	79.59 ± 0.109	0.629 ± 0.009	26496	20.17 ± 0.112	0.093 ± 0.002

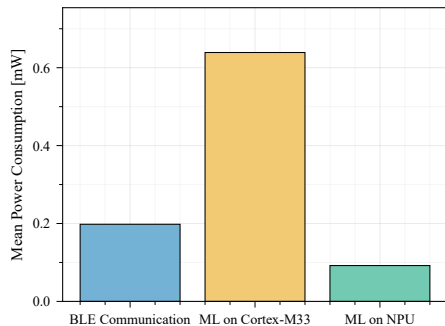


Fig. 3. Comparison of mean power consumption of ML and BLE communication on our experimental sensor device setup.

A. Model Performance and Efficiency

Our analysis of different signal lengths (Tables II and VIII) highlights the critical trade-off between accuracy and efficiency. While using the full 2000 Hz signal provided a marginal accuracy benefit, the associated energy cost was substantial. The selection of a 128-sample input length (42.67 Hz) proved to be an effective compromise, enabling the energy savings shown in Fig. 3 while maintaining high accuracy. The optimal trade-off point, however, remains dependent on the specific use case, acceptable false positive rates, and the device's battery capacity. Quantization introduces another critical trade-off. As shown in Table VI, 8-bit quantization caused noticeable performance degradation (accuracy dropping from 0.9705 to 0.9124). This effect is often pronounced in compact models like ours (15.9K parameters), which lack the high

parameter redundancy that allows larger models to compensate for quantization errors. Consequently, the model is more sensitive to precision loss. While the quantized model still performs well, closing this gap is a subject for future optimization. This could be achieved by integrating quantization constraints directly into the design process, such as through quantization-aware Neural Architecture Search (NAS), to identify architectures inherently more robust to 8-bit precision. Our classification results in Table IV reveal significant performance differences between DL architectures under similar parameter constraints. The CNN's superior performance may be attributed to the nature of the anomalies (e.g., mitral valve prolapse), which often manifest as changes within a cardiac cycle [52], [53]. CNNs excel at detecting these local patterns, whereas longer temporal correlations (captured by LSTMs) may be less critical here. The limited dataset size (405 recordings) likely hindered the transformer, which typically requires more data due to its lack of inductive biases. The results in Table V clearly demonstrate the benefit of fusing ECG and PCG signals, supporting the hypothesis that the electrical (ECG) and mechanical (PCG) information are complementary. Our findings show that even very small DL models can effectively leverage multi-modal data. The efficiency comparison in Table VIII underscores the substantial energy gains achievable by utilizing an NPU. As illustrated in Fig. 3, model inference on the NPU is considerably more efficient than constant BLE communication. In our experiments, the amount of data being constantly transmitted via BLE or processed in our cnn model is roughly equal. By transmitting data only when an anomaly is

detected, the overall energy consumption of the system can be significantly reduced. The efficiency gain (over 53% compared to BLE) provides substantial energy headroom for occasional communication. In a clinical workflow, data corresponding to a detected anomaly must be transmitted for expert review. This requires buffering the N most recent windows used for the majority vote. However, due to the significant downsampling, the memory required for buffering is minimal (128 bytes per signal type per window for the 8-bit quantized model), posing negligible overhead.

B. Limitations and Future Work

A key challenge for continuous monitoring using wearable patches is the susceptibility to motion artifacts and ambient noise. The pipeline presented in this study does not yet include explicit mechanisms to address these factors. The primary goal was to establish the baseline efficiency of on-device ML. For real-world deployment, the pipeline must be extended, potentially by incorporating upstream noise filters or denoising mechanisms. Methods to detect out-of-distribution samples are also necessary. These additions will increase the energy budget, potentially requiring further optimization of the ML model architecture for greater efficiency. This remains a critical area for future work. Furthermore, the model was trained and evaluated only on the "training-a" subset due to the lack of other publicly available datasets containing synchronized ECG and PCG data with cardiovascular disease labels. This limited dataset diversity poses a risk to the generalizability of the findings. To address concerns regarding overfitting and to assess model stability, we employed a rigorous 10-times repeated 5-fold CV strategy. The results demonstrate consistently low standard deviations across all performance metrics, indicating that the model performance is stable and not sensitive to the specific partitioning of the data. Furthermore, as discussed in Section IV-B, the inability to perform patient-level data splitting due to missing metadata means that the reported performance metrics might be optimistic. While the recording-level split mitigates information leakage from highly correlated windows within the same recording, potential correlation from different recordings of the same patient cannot be ruled out. Validation on larger, diverse, and fully annotated datasets is necessary to confirm the clinical robustness of the model.

VII. CONCLUSION

In conclusion, we propose a lightweight CNN model demonstrating competitive classification accuracy on the considered dataset. Through hardware experiments on a microcontroller and an experimental sensor device setup, we validated the model's efficiency. We show that local processing using an NPU and our CNN consumes less energy than continuous data transmission. With this we clearly demonstrate the applicability and advantage of using DL models on resource-constrained medical edge devices. For future research, we envision to extend our analysis of DL in the remote cardiovascular monitoring context to ECG combined with auxiliary data such as accelerometer data to help achieve context awareness. Moreover, crucial aspects of medical monitoring, such as reliability

and robustness can be explored and improved through various further analysis.

APPENDIX

A. Deep Learning Architectures

The MLP model consists of four linear layers with ReLU activations and a final linear layer that maps to the output. The output dimensions of the intermediate layers are 37, 35, 55 and 54. The LSTM model consists of one LSTM layer with a hidden unit size of 61 followed by a final linear layer that maps the output features of the last time step to the output. The transformer model consists of one convolution layer with a kernel size of 14, stride of 3 and output channels of 28 in the beginning to extract patches of the time series followed by two transformer encoder blocks. The encoder blocks each have 28 features and a size of 77 for the token-wise feed-forward network. After the blocks there is an average pooling operation along the time dimension and a final linear layer that maps to the output.

REFERENCES

- [1] British Heart Foundation, "Global heart & circulatory diseases factsheet," accessed: 2024-01-23. [Online]. Available: <https://www.bhf.org.uk/-/media/files/for-professionals/research/heart-statistics/bhf-cvd-statistics-global-factsheet>
- [2] M. J. Stampfer, F. B. Hu, J. E. Manson, E. B. Rimm, and W. C. Willett, "Primary prevention of coronary heart disease in women through diet and lifestyle," *New England Journal of Medicine*, vol. 343, no. 1, pp. 16–22, 2000.
- [3] S. E. Chiuve, M. L. McCullough, F. M. Sacks, and E. B. Rimm, "Healthy lifestyle factors in the primary prevention of coronary heart disease among men: benefits among users and nonusers of lipid-lowering and antihypertensive medications," *Circulation*, vol. 114, no. 2, pp. 160–167, 2006.
- [4] S. Hong, Y. Zhou, J. Shang, C. Xiao, and J. Sun, "Opportunities and challenges of deep learning methods for electrocardiogram data: A systematic review," *Computers in biology and medicine*, vol. 122, p. 103801, 2020.
- [5] W. Chen, Q. Sun, X. Chen, G. Xie, H. Wu, and C. Xu, "Deep learning methods for heart sounds classification: A systematic review," *Entropy*, vol. 23, no. 6, p. 667, 2021.
- [6] Y. LeCun, B. Boser, J. Denker, D. Henderson, R. Howard, W. Hubbard, and L. Jackel, "Handwritten digit recognition with a back-propagation network," *Advances in neural information processing systems*, vol. 2, 1989.
- [7] M. F. R. Ibrahim, T. Alkanat, M. Meijer, A. Schlaefler, and P. Steldinger, "End-to-end multi-modal tiny-cnn for cardiovascular monitoring on sensor patches," in *2024 IEEE International Conference on Pervasive Computing and Communications (PerCom)*. IEEE, 2024, pp. 18–24.
- [8] D. Susič, G. Poglajen, and A. Gradišek, "Identification of decompensation episodes in chronic heart failure patients based solely on heart sounds," *Frontiers in Cardiovascular Medicine*, vol. 9, p. 1009821, 2022.
- [9] B. E. Boser, I. M. Guyon, and V. N. Vapnik, "A training algorithm for optimal margin classifiers," in *Proceedings of the fifth annual workshop on Computational learning theory*, 1992, pp. 144–152.
- [10] J. X. Low and K. W. Choo, "Automatic classification of periodic heart sounds using convolutional neural network," *World Academy Science Engineering and Technology, International Journal of Electrical and Computer Engineering*, vol. 5, pp. 100–105, 2018.
- [11] R. Hettiarachchi, U. Haputhanthri, K. Herath, H. Kariyawasam, S. Munasinghe, K. Wickramasinghe, D. Samarasinghe, A. De Silva, and C. U. Edussooriya, "A novel transfer learning-based approach for screening pre-existing heart diseases using synchronized ecg signals and heart sounds," in *2021 IEEE International Symposium on Circuits and Systems (ISCAS)*. IEEE, 2021, pp. 1–5.
- [12] P. Qi, H. Xu, H. Zhang, J. Tong, and S. Xia, "Residual neural networks based on empirical mode decomposition for mitral regurgitation prediction," *Biomedical Signal Processing and Control*, vol. 86, p. 105265, 2023.

- [13] M. Morshed and S. A. Fattah, "A deep neural network for heart valve defect classification from synchronously recorded ECG and PCG," *IEEE Sensors Letters*, vol. 7, no. 9, pp. 1–4, 2023.
- [14] M. Gjoreski, A. Gradišek, B. Budna, M. Gams, and G. Poglajen, "Machine learning and end-to-end deep learning for the detection of chronic heart failure from heart sounds," *Ieee Access*, vol. 8, pp. 20313–20324, 2020.
- [15] S. Hochreiter and J. Schmidhuber, "Long short-term memory," *Neural computation*, vol. 9, no. 8, pp. 1735–1780, 1997.
- [16] P. Li, Y. Hu, and Z.-P. Liu, "Prediction of cardiovascular diseases by integrating multi-modal features with machine learning methods," *Biomedical Signal Processing and Control*, vol. 66, p. 102474, 2021.
- [17] J. Li, L. Ke, Q. Du, X. Ding, and X. Chen, "Research on the Classification of ECG and PCG Signals Based on BiLSTM-GoogLeNet-DS," *Applied Sciences*, vol. 12, no. 22, p. 11762, 2022.
- [18] H. Zhang, P. Zhang, F. Lin, L. Chao, Z. Wang, F. Ma, and Q. Li, "Co-learning-assisted progressive dense fusion network for cardiovascular disease detection using ECG and PCG signals," *Expert Systems with Applications*, vol. 238, p. 122144, 2024.
- [19] W. P. Li, J. H. Chuah, G. J. Tan, C. Liu, and H.-N. Ting, "A progressive attention-based cross-modal fusion network for cardiovascular disease detection using synchronized electrocardiogram and phonocardiogram signals," *PeerJ Computer Science*, vol. 11, p. e3038, 2025.
- [20] C. Thomae and A. Dominik, "Using deep gated RNN with a convolutional front end for end-to-end classification of heart sound," in *2016 Computing in Cardiology Conference (CinC)*. IEEE, 2016, pp. 625–628.
- [21] N. Gautam, S. N. Ghanta, J. Mueller, M. Mansour, Z. Chen, C. Puente, Y. M. Ha, T. Tarun, G. Dhar, K. Sivakumar *et al.*, "Artificial intelligence, wearables and remote monitoring for heart failure: current and future applications," *Diagnostics*, vol. 12, no. 12, p. 2964, 2022.
- [22] C. Krittanawong, A. J. Rogers, K. W. Johnson, Z. Wang, M. P. Turakhia, J. L. Halperin, and S. M. Narayan, "Integration of novel monitoring devices with machine learning technology for scalable cardiovascular management," *Nature Reviews Cardiology*, vol. 18, no. 2, pp. 75–91, 2021.
- [23] N. Alugubelli, H. Abuissa, and A. Roka, "Wearable devices for remote monitoring of heart rate and heart rate variability—what we know and what is coming," *Sensors*, vol. 22, no. 22, p. 8903, 2022.
- [24] L. Neri, M. T. Oberdier, K. C. van Abeelen, L. Menghini, E. Tumarkin, H. Tripathi, S. Jaipalli, A. Orro, N. Paolucci, I. Gallelli *et al.*, "Electrocardiogram monitoring wearable devices and artificial-intelligence-enabled diagnostic capabilities: a review," *Sensors*, vol. 23, no. 10, p. 4805, 2023.
- [25] M. Moshawrab, M. Adda, A. Bouzouane, H. Ibrahim, and A. Raad, "Smart wearables for the detection of cardiovascular diseases: a systematic literature review," *Sensors*, vol. 23, no. 2, p. 828, 2023.
- [26] S. Lee, Y. Chu, J. Ryu, Y. J. Park, S. Yang, and S. B. Koh, "Artificial intelligence for detection of cardiovascular-related diseases from wearable devices: a systematic review and meta-analysis," *Yonsei medical journal*, vol. 63, no. Suppl, p. S93, 2022.
- [27] H. D. M. Ribeiro, A. Arnold, J. P. Howard, M. J. Shun-Shin, Y. Zhang, D. P. Francis, P. B. Lim, Z. Whinnett, and M. Zolgharni, "ECG-based real-time arrhythmia monitoring using quantized deep neural networks: A feasibility study," *Computers in Biology and Medicine*, vol. 143, p. 105249, 2022.
- [28] S. Ran, X. Yang, M. Liu, Y. Zhang, C. Cheng, H. Zhu, and Y. Yuan, "Homecare-oriented ECG diagnosis with large-scale deep neural network for continuous monitoring on embedded devices," *IEEE Transactions on Instrumentation and Measurement*, vol. 71, pp. 1–13, 2022.
- [29] J. Lu, D. Liu, Z. Liu, X. Cheng, L. Wei, C. Zhang, X. Zou, and B. Liu, "Efficient hardware architecture of convolutional neural network for ECG classification in wearable healthcare device," *IEEE Transactions on Circuits and Systems I: Regular Papers*, vol. 68, no. 7, pp. 2976–2985, 2021.
- [30] Y.-T. Hsieh, K. Anjum, and D. Pompili, "Ultra-low power analog folded neural network for cardiovascular health monitoring," *IEEE Journal of Biomedical and Health Informatics*, 2024.
- [31] Z. Jin, Y. Sun, and A. C. Cheng, "Predicting cardiovascular disease from real-time electrocardiographic monitoring: An adaptive machine learning approach on a cell phone," in *2009 Annual International Conference of the IEEE Engineering in Medicine and Biology Society*. IEEE, 2009, pp. 6889–6892.
- [32] Z. Jin, J. Oresko, S. Huang, and A. C. Cheng, "HeartToGo: a personalized medicine technology for cardiovascular disease prevention and detection," in *2009 IEEE/NIH Life Science Systems and Applications Workshop*. IEEE, 2009, pp. 80–83.
- [33] C. Liu, D. Springer, Q. Li, B. Moody, R. A. Juan, F. J. Chorro, F. Castells, J. M. Roig, I. Silva, A. E. Johnson *et al.*, "An open access database for the evaluation of heart sound algorithms," *Physiological measurement*, vol. 37, no. 12, p. 2181, 2016.
- [34] A. L. Goldberger, L. A. Amaral, L. Glass, J. M. Hausdorff, P. C. Ivanov, R. G. Mark, J. E. Mietus, G. B. Moody, C.-K. Peng, and H. E. Stanley, "PhysioBank, PhysioToolkit, and PhysioNet: components of a new research resource for complex physiologic signals," *circulation*, vol. 101, no. 23, pp. e215–e220, 2000.
- [35] M. Sandler, A. Howard, M. Zhu, A. Zhmoginov, and L.-C. Chen, "Mobilenetv2: Inverted residuals and linear bottlenecks," in *Proceedings of the IEEE conference on computer vision and pattern recognition*, 2018, pp. 4510–4520.
- [36] A. Howard, M. Sandler, G. Chu, L.-C. Chen, B. Chen, M. Tan, W. Wang, Y. Zhu, R. Pang, V. Vasudevan *et al.*, "Searching for mobilenetv3," in *Proceedings of the IEEE/CVF international conference on computer vision*, 2019, pp. 1314–1324.
- [37] F. Rosenblatt, "The perceptron: a probabilistic model for information storage and organization in the brain," *Psychological review*, vol. 65, no. 6, p. 386, 1958.
- [38] A. Vaswani, N. Shazeer, N. Parmar, J. Uszkoreit, L. Jones, A. N. Gomez, Ł. Kaiser, and I. Polosukhin, "Attention is all you need," *Advances in neural information processing systems*, vol. 30, 2017.
- [39] A. Paszke, S. Gross, F. Massa, A. Lerer, J. Bradbury, G. Chanan, T. Killeen, Z. Lin, N. Gimelshein, L. Antiga *et al.*, "Pytorch: An imperative style, high-performance deep learning library," *Advances in neural information processing systems*, vol. 32, 2019.
- [40] I. Loshchilov and F. Hutter, "Decoupled weight decay regularization," *arXiv preprint arXiv:1711.05101*, 2017.
- [41] T. Akiba, S. Sano, T. Yanase, T. Ohta, and M. Koyama, "Optuna: A next-generation hyperparameter optimization framework," in *The 25th ACM SIGKDD International Conference on Knowledge Discovery & Data Mining*, 2019, pp. 2623–2631.
- [42] J. K. Blitzstein and J. Hwang, *Introduction to probability*. Crc Press, 2019.
- [43] V. Sovrasov. (2018–2024) ptflops: a flops counting tool for neural networks in pytorch framework. [Online]. Available: <https://github.com/sovrasov/flops-counter.pytorch>
- [44] B. Jacob, S. Kligys, B. Chen, M. Zhu, M. Tang, A. Howard, H. Adam, and D. Kalenichenko, "Quantization and training of neural networks for efficient integer-arithmetic-only inference," in *Proceedings of the IEEE conference on computer vision and pattern recognition*, 2018, pp. 2704–2713.
- [45] NXP Semiconductors, "Evaluation Kit for MCX N94x MCUs," accessed: 2025-01-31. [Online]. Available: <https://www.nxp.com/design/design-center/development-boards-and-designs/MCX-N9XX-EVK>
- [46] ARM, "Cortex-M33," accessed: 2025-01-31. [Online]. Available: <https://developer.arm.com/Processors/Cortex-M33>
- [47] L. Bamberg, F. Minnella, R. Bosio, F. Ottati, Y. Wang, J. Lee, L. Lavagno, and A. Fuks, "eIQ Neutron: Redefining Edge-AI Inference with Integrated NPU and Compiler Innovations," *arXiv preprint arXiv:2509.14388*, 2025.
- [48] NXP Semiconductors, "MCU-Link Pro Debug Probe," accessed: 2025-01-31. [Online]. Available: <https://www.nxp.com/design/design-center/software/software-library/mcu-link-pro-debug-probe:MCU-LINK-PRO>
- [49] *MCX Nx4x Power Management User Guide*, Rev. 2.0 ed., NXP Semiconductors, Eindhoven, Netherlands, 2024.
- [50] NXP Semiconductors, "NHS52S04: Ultra-Low-Power Bluetooth® Low Energy Solution With Arm® Cortex®-M33 TrustZone® for Medical IoT," accessed: 2025-01-31. [Online]. Available: <https://www.nxp.com/products/NHS52S04>
- [51] Sencure, "SNCE800 Series™," accessed: 2025-01-31. [Online]. Available: <https://sencure.com/technology/>
- [52] Z. R. Bhutto, J. T. Barron, P. R. Liebson, E. F. Uretz, and J. E. Parrillo, "Electrocardiographic abnormalities in mitral valve prolapse," *The American journal of cardiology*, vol. 70, no. 2, pp. 265–266, 1992.
- [53] Y. Birnbaum, J. M. Wilson, M. Fiol, A. B. de Luna, M. Eskola, and K. Nikus, "Ecg diagnosis and classification of acute coronary syndromes," *Annals of noninvasive electrocardiology*, vol. 19, no. 1, pp. 4–14, 2014.